Vortex Lattices in Active Nematics with Periodic Obstacle Arrays

Cody D. Schimming,* C. J. O. Reichhardt, and C. Reichhardt
Theoretical Division and Center for Nonlinear Studies, Los Alamos National Laboratory, Los Alamos, New Mexico 87545, USA

(Received 14 September 2023; accepted 16 November 2023; published 4 January 2024)

We numerically model a two-dimensional active nematic confined by a periodic array of fixed obstacles. Even in the passive nematic, the appearance of topological defects is unavoidable due to planar anchoring by the obstacle surfaces. We show that a vortex lattice state emerges as activity is increased, and that this lattice may be tuned from "ferromagnetic" to "antiferromagnetic" by varying the gap size between obstacles. We map the rich variety of states exhibited by the system as a function of distance between obstacles and activity, including a pinned defect state, motile defects, the vortex lattice, and active turbulence. We demonstrate that the flows in the active turbulent phase can be tuned by the presence of obstacles, and explore the effects of a frustrated lattice geometry on the vortex lattice phase.

DOI: 10.1103/PhysRevLett.132.018301

Active nematics are a class of active fluids whose microscopic constituents are anisotropic and exert dipolar forces [1,2]. Examples of such systems include cytoskeletal filaments with molecular motors [3], cellular tissues [4], suspensions of bacteria in nematic liquid crystals [5,6], and soil bacteria [7]. One of the key features of active nematics is that in many cases the dynamics can be described by the motion of defects with different topological charges [3,8–10]. There is growing interest in developing methods to control active nematic defect dynamics and flows, such as by applying external fields [11], introducing anisotropic substrates [12,13], or imposing a geometric confinement of the material [14,15].

In systems with well-defined length scales such as the average distance between topological defects, new ordered phases can arise upon coupling to a periodic substrate [16], as observed for vortices in superconductors [17] and Bose-Einstein condensates [18], ordering of surfaces [19], cold atoms [20], and colloids [21,22]. Active nematics are another system in which commensuration effects can arise; however, due to their nonequilibrium nature, it should be possible for dynamical commensuration effects to appear as well. Here, we examine the effects of geometric confinement on active nematics induced by a periodic array of fixed obstacles for varied activity levels and obstacle sizes. Previous theoretical and experimental studies of active nematic confinement typically employed an external boundary as a confining structure, resulting in a channel, circular disk, or annular geometry [14,23–30]. As the system size and active force magnitude are varied, such systems can exhibit anomalous flow states such as dancing topological defects or systemwide circulation [14,24–26]. Relatively few studies have addressed the effects of fixed, embedded obstacles on the active nematic flow state; however, recent experiments have successfully produced active nematics in obstacle laden environments [31,32].

Motivated by the recent experimental work, we use a minimal, active nematic continuum model to simulate an array of obstacles that separates the system into interacting circular domains where the obstacle shape makes the formation of topological defects unavoidable. We show that a variety of phases appear, including a low active force state where the defects remain pinned to the obstacles, a motile defect state, and an intermediate activity state where the flow organizes into a lattice of vortices. By varying the obstacle size, we can tune the vortex lattice from "ferromagnetic," in which all vortices have the same chirality, to "antiferromagnetic," in which each nearest neighbor vortex pair is of opposite chirality. To our knowledge, this is the first report of a ferromagnetic vortex lattice state in active nematics. We compare the active turbulent phase in systems with and without obstacles and find that the fluid flow slows as the obstacles increase in size, while the directional distribution of the fluid velocity becomes peaked along diagonal lattice directions. Finally, we explore the effects of lattice frustration by simulating the active nematic on a triangular lattice. Our findings provide an experimentally viable method for controlling and tuning vortex lattices and flows in active nematics.

We model a two-dimensional active nematic using a well-documented continuum model that has been shown to capture the key features of experimental active nematics [2,33]. In our dimensionless equations [34], the units of length and time are the nematic correlation length ξ and the nematic relaxation time σ. The nematic state is captured by the tensor order parameter $\mathbf{Q} = S[\mathbf{n} \otimes \mathbf{n} - (1/2)\mathbf{I}]$ where S is the scalar order parameter indicating the local degree of alignment and $\mathbf{n}$ is the director, giving the local direction of orientation. The evolution of $\mathbf{Q}$ is given by

$$\frac{\partial \mathbf{Q}}{\partial t} + (\mathbf{v} \cdot \nabla)\mathbf{Q} - \mathbf{S} = -\frac{\delta F}{\delta \mathbf{Q}}, \tag{1}$$

where F is the Landau-de Gennes free energy with one elastic constant [35], $\mathbf{S}$ is a generalized tensor advection with flow alignment parameter $\lambda = 1$ [36], and $\mathbf{v}$ is the fluid velocity. The free energy is such that the passive liquid crystal is in the nematic phase. We assume low Reynolds number flow, so the fluid velocity is given by the Stokes equation:

$$\nabla^2 \mathbf{v} = \nabla p + \alpha \nabla \cdot \mathbf{Q}, \qquad \nabla \cdot \mathbf{v} = 0, \tag{2}$$

where p is the fluid pressure, and the last term is an addition to the usual Stokes equation that models an active force of dimensionless strength α. The divergence free condition models incompressible flows.

Equations (1) and (2) are discretized in space and time and solved using the MATLAB/C++ package FELICITY [34,37]. We consider domains with an array of astroid shaped obstacles, as shown in Fig. 1(a). The obstacles effectively create circular domains that overlap over a distance d between obstacles. We vary d from 1 to 10 while fixing the distance between obstacle centers to $a = 14$ so that the overall system size remains constant. The limit $d = 0$ gives individual, noninteracting circular domains. We employ periodic boundary conditions on the side edges of the domain, while for the obstacles we impose strong planar anchoring for $\mathbf{Q}$ and no-slip conditions for $\mathbf{v}$. The shape of the inclusions and the strong planar anchoring necessitate the formation of topological defects, or points where the nematic director is singular. Specifically, there must be a total topological charge (winding number) of $+N$ for N obstacles because each obstacle carries a charge of -1. In the limit $d = a$ the obstacles no longer exist and the total topological charge must be zero. Therefore, when $d < a$, topological defects inherently exist in the system even in the passive state with $\alpha = 0$. We discuss the role of obstacle shape in the Supplemental Material [34] and note that our results should hold as long as the anchoring is strong enough to induce formation of topological defects [34].

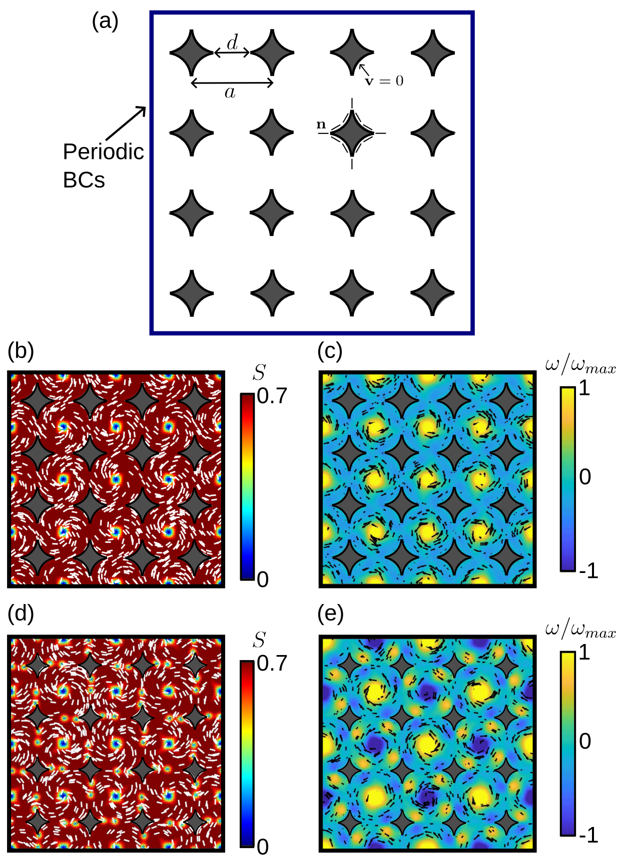

FIG. 1. (a) Schematic of the computational domain with a periodic array of astroid shaped obstacles summarizing the boundary conditions on the obstacles and domain edges. (b), (c) "Ferromagnetic" vortex lattice state at $d = 2$ and $\alpha = 1.8$. (b) Nematic scalar order parameter S where white lines indicate the director $\mathbf{n}$. The points where $S = 0$ are topological defects. (c) Fluid vorticity with black arrows showing the velocity field. (d) S and (e) $\omega/\omega_{\max}$ for an "antiferromagnetic" vortex lattice state at $d = 6$ and $\alpha = 1.5$ [34].

Upon increasing α for various obstacle sizes, we typically find three qualitative transitions. At zero and small activity, the topological defects are pinned to the obstacles. As the activity is increased, the defects begin to unpin and move from obstacle to obstacle with little to no unbinding of new defects. When activity is further increased, a central vortex forms in each circular domain with two $+1/2$ topological charge defects encircling one another, as has been shown previously for individual circular domains [14,26,30]. At higher activities the $+1/2$ defects merge, and a stable $+1$ spiral defect forms in the domain center. The stability of the spiral defect is due to the flow aligning nature of the nematic, and if $\lambda = 0$ the spirals and vortices are no longer stable [34,38]. Figures 1(b)–1(e) show examples of the nematic order parameter and velocity field in the vortex lattice state, which can have either ferromagnetic or antiferromagnetic order. At still higher activities the central vortex in each domain is no longer stable, and an active turbulent phase persists in which defects are constantly unbinding and annihilating.

To better quantify the transitions, we map our system to a lattice of vortex "spins" by measuring the average vorticity in a circle of diameter $a/2$ at the center of each circular domain. The spins are then indexed by their lattice position s_i. Figures 2(a)–2(c) show plots of $\langle |s_i| \rangle_{i,t}$, where $\langle \cdot \rangle_{i,t}$ denotes an average over lattice sites and time, as a function of activity for obstacle gaps $d = 4$, $d = 6$, and $d = 8$. The transition to the vortex lattice state is marked by a jump followed by a linear increase in $\langle |s_i| \rangle_{i,t}$. A second transition is marked by an abrupt decrease in $\langle |s_i| \rangle_{i,t}$ which remains roughly constant. This is the active turbulent phase.

We first focus on the vortex lattice phase, which can have either "ferromagnetic" or "antiferromagnetic" order that we quantify with the spin-spin correlation function

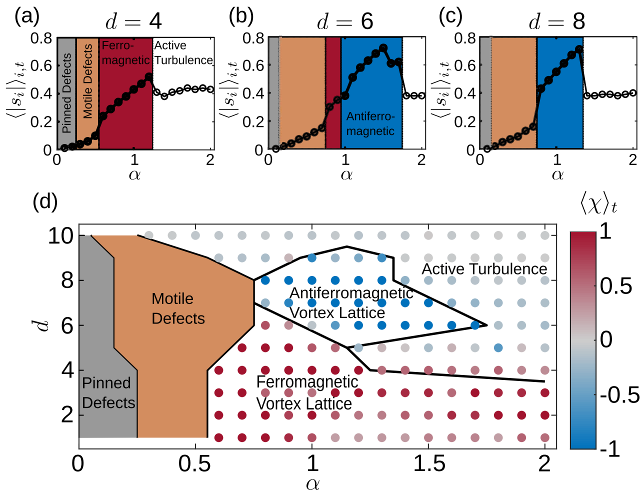

FIG. 2. (a)–(c) Average vortex "spin" $\langle|s_i|\rangle_{i,t}$ as a function of activity α for obstacle gaps (a) $d = 4$, (b) $d = 6$, and (c) $d = 8$. Colors indicate the phase identity. (d) Phase diagram as a function of d vs α, where dot color indicates the value of the time-averaged spin-spin correlation function $\langle\chi\rangle_t$. $\langle\chi\rangle_t$ is not well-defined in the pinned defect or motile defect phases.

$$\chi = \frac{\sum_{\langle i,j\rangle} s_i s_j}{\sum_{\langle i,j\rangle} |s_i s_j|}, \tag{3}$$

where $\sum_{\langle i,j\rangle}$ denotes a sum over nearest neighbor pairs. For perfectly ferromagnetic (antiferromagnetic) order $\chi = 1$ ($\chi = -1$). In Fig. 2(d) we plot the phase boundaries as well as $\langle\chi\rangle_t$ as a function of activity and obstacle gap in both the vortex lattice and active turbulence regimes. We do not define χ for small activities since the central vortices, and hence spins, are not well-established in the pinned defect and motile defect phases. As the obstacle gap increases, there is a window of activity values where the vortex lattice abruptly transitions from ferromagnetic to antiferromagnetic. In this window, the obstacle size can be used to tune the vortex lattice state. To check the ferromagnetic-antiferromagnetic transition for hysteresis we fix $d = 6$ and sweep the activity up and down between $\alpha = 0.8$ and $\alpha = 1.4$, finding minimal hysteresis as indicated by the plot of $\chi(t)$ in Fig. SX.

For large obstacle gaps the vortex lattice phase disappears, and only active turbulence occurs. At the transition from vortex lattice to active turbulence, $\langle\chi\rangle_t$ decreases in size but typically maintains the same sign, indicating that vestigial ferromagnetic or antiferromagnetic order persists until α becomes large enough that $\langle\chi\rangle_t \to 0$.

In previous work on active nematics, a one-dimensional antiferromagnetic vortex lattice was observed in channel confinement geometries [24], while numerical predictions indicate that a two-dimensional antiferromagnetic vortex lattice should appear in systems with large enough substrate friction [39,40]. In our system, we assume zero substrate friction so the vortices are stabilized purely by geometric confinement, but we show in the Supplemental Material [34] that the vortex lattice phase is stable against moderate degrees of substrate friction, consistent with recent work on circularly confined systems [30,34]. We find both ferromagnetic and antiferromagnetic vortex lattices depending on the values of d and α, and to our knowledge, a ferromagnetic vortex lattice has not previously been observed or predicted in active nematics.

Vortex lattices can also form in bacterial suspensions confined by pillar arrays, but in that system, hydrodynamic interactions are the dominant ordering mechanism, and therefore the vortex lattice typically has antiferromagnetic ordering [41,42]. In contrast, in the active nematic considered here, a competition between elastic and active forces determines the vortex lattice structure. The nematic elastic force favors uniform alignment of the director, so domains with opposite chirality incur an elastic energy penalty since the director changes at the domain boundary. Thus, elastic interactions promote ferromagnetic order.

The transitions to antiferromagnetic order and active turbulence may be explained by the competition between elastic and active forces and a hierarchy of length scales. The active nematic length scale $\xi_a \propto 1/\sqrt{\alpha}$ sets the defect density of a bulk active nematic system [2]. For a given obstacle size, there is an effective length scale associated with the circular domains $R_{\rm eff}$. If $\xi_a \lesssim R_{\rm eff}$, there is enough space to nucleate defects and reach the optimal defect density, so the system transitions to an active turbulent state, but there is also a gap length scale d associated with the obstacles. In Fig. 1(d) the antiferromagnetic vortex lattice contains extra $\pm 1/2$ defect pairs that sit in the obstacle gaps and mediate the change in chirality between central vortices. If $\xi_a \gtrsim d$, the active force is too weak to stabilize a defect pair in the gap. On the other hand, if $d \gtrsim \xi_a \gtrsim R_{\rm eff}$, the vortex lattice phase is stable since an extra defect pair can nucleate in the gaps to mediate the antiferromagnetic vortex order. When $d < R_{\rm eff}$, this hierarchy of length scales cannot occur, explaining why antiferromagnetic vortex order is absent for small d. By measuring both the elastic energy and the active energy injected per simulated time step, we find that at the ferromagnetic to antiferromagnetic transition, the active energy becomes dominant and stabilizes the opposing chiralities of neighboring domains, as shown in Fig. S2.

The active turbulent phase that occurs for large α is associated with a sharp decrease in $\langle|s_i|\rangle_{i,t}$ (Fig. 2). We can also measure the average number of defects $\langle N_D\rangle_t$ to detect the transition (see the Supplemental Material for details on how this and other measures are computed [34,43,44]). In the vortex lattice phase, $\langle N_D\rangle_t$ is roughly constant, while in active turbulence $\langle N_D\rangle_t$ grows linearly with α (Fig. S3). Both measures are consistent with one another, and we use them to determine the boundary shown in Fig. 2 between the motile defect phase and active turbulence for large d.

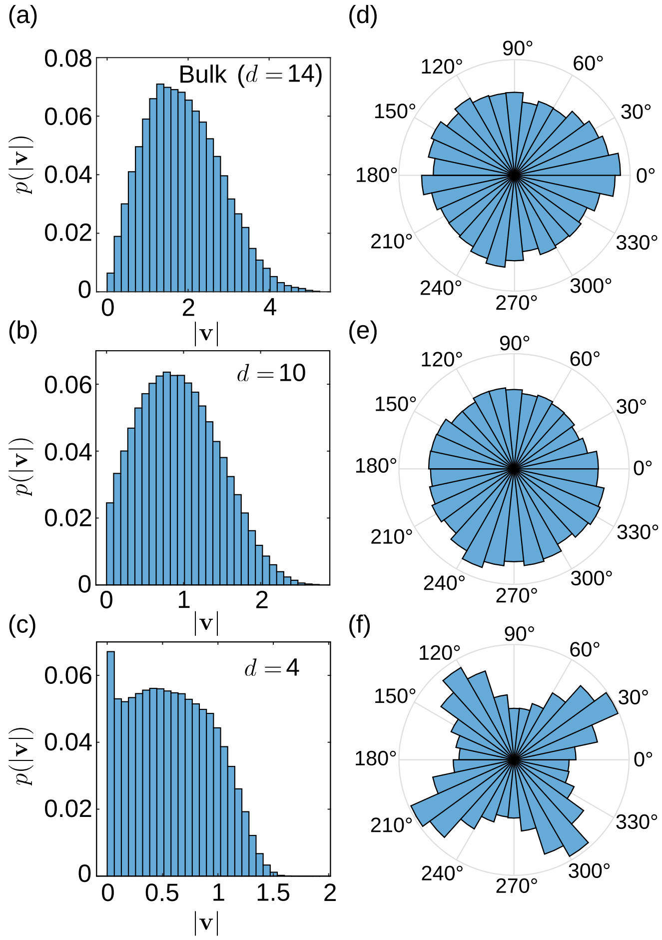

FIG. 3. Flow velocity distributions in the active turbulent phase with $\alpha = 1.5$ and various obstacle gap sizes. (a)–(c) Distributions of $|\mathbf{v}|$ for (a) a bulk system with no obstacles, (b) obstacle gap $d = 10$, and (c) obstacle gap $d = 4$. (d)–(e) Velocity direction distributions $p(\theta_v)$ for (d) a bulk system with no obstacles, (e) obstacle gap $d = 10$, and (f) obstacle gap $d = 4$.

It is instructive to compare the active turbulent phase of the obstacle array system with the $d = a$ bulk system free of obstacles. While the flows in all systems become decorrelated over long timescales (Fig. S4), the flow velocity distributions $p(|\mathbf{v}|)$ vary. In Figs. 3(a)–3(c) we plot $p(|\mathbf{v}|)$ for systems with $\alpha = 1.5$ at $d = 14$ (the bulk system), $d = 10$, and $d = 4$. Figure 3(a) indicates that $p(|\mathbf{v}|)$ has a two-dimensional Maxwell-Boltzmann distribution with a maximum weight that shifts toward $|\mathbf{v}| = 0$ as the obstacle size increases and d becomes smaller. This is a natural consequence of the fact that the obstacles have no-slip conditions and their surface area increases as d decreases. The corresponding velocity direction distributions $p(\theta_v)$ in Figs. 3(d)–3(f), where $\theta_v = \tan^{-1}(v_y/v_x)$, show an isotropic distribution for small obstacles ($d = 10$) that is nearly identical to $p(\theta_v)$ for the bulk system. For larger obstacles, $p(\theta_v)$ becomes anisotropic and peaks along the lattice diagonals. These velocity statistics suggest that immersed obstacles can provide control over the flows even in the active turbulent phase, which could contribute to the development of novel microfluidic devices composed of active fluids.

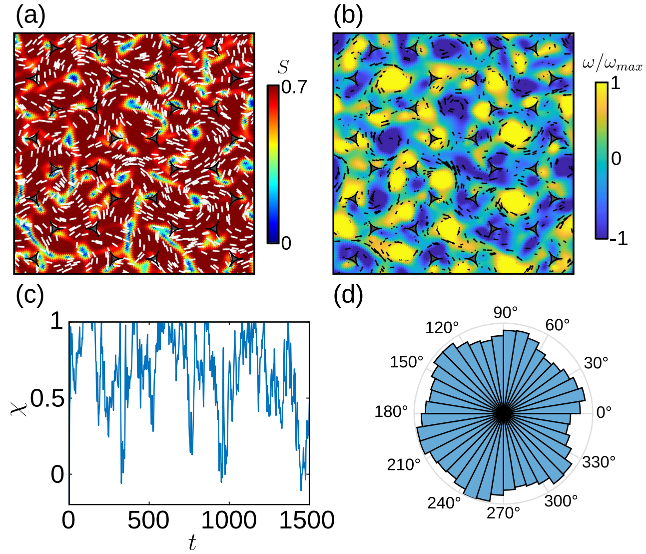

FIG. 4. Active nematic system in a honeycomb lattice of concave triangular obstacles. (a) Time snapshot of the nematic configuration at $a = 8$, $d = 4$, and $\alpha = 2$ with color given by the scalar order parameter S and white lines indicating the nematic director $\mathbf{n}$. (b) The corresponding vorticity (color) and flow velocity (black arrows). (c) Spin-spin correlation function χ vs time t. (d) Velocity direction distribution $p(\theta_v)$.

Finally, we simulate the active nematic in a domain constrained by a honeycomb lattice of concave, triangular obstacles similar to those used in recent experiments [31]. Here, the obstacles introduce a triangular lattice of circular domains. An example nematic configuration and flow profile is shown in Figs. 4(a) and 4(b). In order to promote antiferromagnetic ordering, we place the system just outside the ferromagnetic vortex lattice phase for this geometry: $a = 8$, $d = 4$, and $\alpha = 2$; however, a triangular lattice is frustrated, and the checkerboard pattern that occurs in square lattices is not possible, but is replaced by many degenerate ground states [45,46]. As a result we find a primarily ferromagnetic state in which the competition between elastic and active forces results in constantly flipping spins and the formation of a dynamical state similar to active turbulence. In Fig. 4(c) we plot $\chi(t)$ over the course of a simulation. There are multiple time intervals where $\chi = 1$, indicating a perfectly ferromagnetic vortex lattice; however, spin flips generated by the unbinding of new defects constantly reduce χ, which sometimes becomes negative. While the dynamics resemble active turbulence, we argue that they are actually closer to those of the vortex lattice state in the square lattice with $d = 6$ and $\alpha = 0.9$, in which the underlying vortex lattice order is ferromagnetic, but defect unbinding pushes the system toward antiferromagnetic order. We show in Fig. S5 that the χ-χ temporal autocorrelation function for the frustrated triangular lattice is similar to that of the square lattice with $d = 6$ and $\alpha = 0.9$. In both systems, but unlike an active turbulent system, χ is correlated over long times, indicating that spins and spin flips are also correlated over time. In Fig. 4(d) we show that $p(\theta_v)$ peaks at the six diagonals of the lattice. We expect the peaks to become more prominent as the obstacle size increases.

Conclusion.—We have numerically studied the effects on active nematics of fixed periodic astroid shaped obstacles with planar nematic anchoring. As a function of activity and obstacle size, we find a wide variety of phases, including a pinned defect phase, motile defect regime, and a vortex lattice phase that can be tuned from ferromagnetic to antiferromagnetic. There is an active turbulent phase that displays unique anisotropic velocity distributions at high activities, suggesting a new method to control active turbulence with obstacles. We also find that an antiferromagnetic vortex lattice on a triangular lattice exhibits an active frustrated state. Our system should be experimentally realizable using existing approaches for creating obstacles in active nematic systems [31,32]. Future directions are to consider obstacle shapes that stabilize other kinds of topological defects (see the Supplemental Material and Fig. S6 [34]). Also, different lattices may yield even more exotic flow states, which opens the prospect of flow control in active nematics using obstacles.

This work was supported by the U.S. Department of Energy through the Los Alamos National Laboratory. Los Alamos National Laboratory is operated by Triad National Security, LLC, for the National Nuclear Security Administration of the U.S. Department of Energy (Contract No. 89233218CNA000001).

[*]cschim@lanl.gov

[1] M. C. Marchetti, J. F. Joanny, S. Ramaswamy, T. B. Liverpool, J. Prost, M. Rao, and R. A. Simha, Hydrodynamics of soft active matter, Rev. Mod. Phys. **85**, 1143 (2013).

[2] A. Doostmohammadi, J. Ignés-Mullol, J. M. Yeomans, and F. Sagués, Active nematics, Nat. Commun. **9**, 3246 (2018).

[3] T. Sanchez, D. T. N. Chen, S. J. DeCamp, M. Heymann, and Z. Dogic, Spontaneous motion in hierarchically assembled active matter, Nature (London) **491**, 431 (2012).

[4] T. B. Saw, A. Doostmohammadi, V. Nier, L. Kocgozlu, S. Thampi, Y. Toyama, P. Marcq, C. T. Lim, J. M. Yeomans, and B. Ladoux, Topological defects in epithelia govern cell death and extrusion, Nature (London) **544**, 212 (2017).

[5] S. Zhou, A. Sokolov, O. D. Lavrentovich, and I. S. Aranson, Living liquid crystals, Proc. Natl. Acad. Sci. U.S.A. **111**, 1265 (2014).

[6] M. M. Genkin, A. Sokolov, O. D. Lavrentovich, and I. S. Aranson, Topological defects in a living nematic ensnare swimming bacteria, Phys. Rev. X **7**, 011029 (2017).

[7] K. Copenhagen, R. Alert, N. S. Wingreen, and J. W. Shaevitz, Topological defects promote layer formation in *Myxococcus xanthus* colonies, Nat. Phys. **17**, 211 (2021).

[8] S. J. DeCamp, G. S. Redner, A. Baskaran, M. F. Hagan, and Z. Dogic, Orientational order of motile defects in active nematics, Nat. Mater. **14**, 1110 (2015).

[9] L. Giomi, M. J. Bowick, P. Mishra, R. Sknepnek, and M. C. Marchetti, Defect dynamics in active nematics, Phil. Trans. R. Soc. A **372**, 20130365 (2014).

[10] S. Shankar and M. C. Marchetti, Hydrodynamics of active defects: From order to chaos to defect ordering, Phys. Rev. X **9**, 041047 (2019).

[11] P. Guillamat, J. Ignés-Mullol, and F. Sagués, Control of active liquid crystals with a magnetic field, Proc. Natl. Acad. Sci. U.S.A. **113**, 5498 (2016).

[12] P. Guillamat, J. Ignés-Mullol, S. Shankar, M. C. Marchetti, and F. Sagués, Probing the shear viscosity of an active nematic film, Phys. Rev. E **94**, 060602(R) (2016).

[13] K. Thijssen, L. Metselaar, J. M. Yeomans, and A. Doostmohammadi, Active nematics with anisotropic friction: The decisive role of the flow aligning parameter, Soft Matter **16**, 2065 (2020).

[14] A. Opathalage, M. M. Norton, M. P. N. Juniper, B. Langeslay, S. A. Aghvami, S. Fraden, and Z. Dogic, Self-organized dynamics and the transition to turbulence of confined active nematics, Proc. Natl. Acad. Sci. U.S.A. **116**, 4788 (2019).

[15] K. Thijssen, D. A. Khaladj, S. A. Aghvami, M. A. Gharbi, S. Fraden, J. M. Yeomans, L. S. Hirst, and T. N. Shendruk, Submersed micropatterned structures control active nematic flow, topology, and concentration, Proc. Natl. Acad. Sci. U.S.A. **118**, e2106038118 (2021).

[16] P. Bak, Commensurate phases, incommensurate phases and the devil's staricase, Rep. Prog. Phys. **45**, 587 (1982).

[17] K. Harada, O. Kamimura, H. Kasai, T. Matsuda, A. Tonomura, and V. V. Moshchalkov, Direct observation of vortex dynamics in superconducting films with regular arrays of defects, Science **274**, 1167 (1996).

[18] S. Tung, V. Schweikhard, and E. A. Cornell, Observation of vortex pinning in Bose-Einstein condensates, Phys. Rev. Lett. **97**, 240402 (2006).

[19] S. N. Coppersmith, D. S. Fisher, B. I. Halperin, P. A. Lee, and W. F. Brinkman, Dislocations and the commensurate-incommensurate transition in two dimensions, Phys. Rev. B **25**, 349 (1982).

[20] I. Bloch, Ultracold quantum gases in optical lattices, Nat. Phys. **1**, 23 (2005).

[21] A. Ortiz-Ambriz and P. Tierno, Engineering of frustration in colloidal artificial ices realized on microfeatured grooved lattices, Nat. Commun. **7**, 10575 (2016).

[22] T. Bohlein, J. Mikhael, and C. Bechinger, Observation of kinks and antikinks in colloidal monolayers driven across ordered surfaces, Nat. Mater. **11**, 126 (2012).

[23] H. Wioland, F. G. Woodhouse, J. Dunkel, J. O. Kessler, and R. E. Goldstein, Confinement stabilizes a bacterial suspension into a spiral vortex, Phys. Rev. Lett. **110**, 268102 (2013).

[24] T. N. Shendruk, A. Doostmohammadi, K. Thijssen, and J. M. Yeomans, Dancing disclinations in confined active nematics, Soft Matter **13**, 3853 (2017).

[25] K.-T. Wu, J. B. Hishamunda, D. T. N. Chen, S. J. DeCamp, Y.-W. Chang, A. Fernández-Nieves, S. Fraden, and Z. Dogic, Transition from turbulent to coherent flows in confined three-dimensional active fluids, Science **355**, eaal1979 (2017).

[26] M. M. Norton, A. Baskaran, A. Opathalage, B. Langeslay, S. Fraden, A. Baskaran, and M. F. Hagan, Insensitivity of active nematic liquid crystal dynamics to topological constraints, Phys. Rev. E **97**, 012702 (2018).

[27] S. Chandragiri, A. Doostmohammadi, J. M. Yeomans, and S. P. Thampi, Flow states and transitions of an active nematic in a three-dimensional channel, Phys. Rev. Lett. **125**, 148002 (2020).

[28] J. Hardoüin, J. Laurent, T. Lopez-Leon, J. Ignés-Mullol, and F. Sagués, Active microfluidic transport in two-dimensional handlebodies, Soft Matter **16**, 9230 (2020).

[29] M. Varghese, A. Baskaran, M. F. Hagan, and A. Baskaran, Confinement-induced self-pumping in 3D active fluids, Phys. Rev. Lett. **125**, 268003 (2020).

[30] C. D. Schimming, C. J. O. Reichhardt, and C. Reichhardt, Friction-mediated phase transition in confined active nematics, Phys. Rev. E **108**, L012602 (2023).

[31] N. Figueroa-Morales, M. M. Genkin, A. Sokolov, and I. S. Aranson, Non-symmetric pinning of topological defects in living liquid crystals, Commun. Phys. **5**, 301 (2022).

[32] I. Vélez-Cerón, P. Guillamat, F. Sagués, and J. Ignés-Mullol, Probing active nematics with in-situ microfabricated elastic inclusions, arXiv:2307.11587.

[33] D. Marenduzzo, E. Orlandini, M. E. Cates, and J. M. Yeomans, Steady-state hydrodynamic instabilities of active liquid crystals: Hybrid lattice boltzmann simulations, Phys. Rev. E **76**, 031921 (2007).

[34] See Supplemental Material at http://link.aps.org/supplemental/10.1103/PhysRevLett.132.018301 for details on the continuum model, numerical method, measures used to produce the phase diagram, a discussion of the potential effects of other model parameters, and Supplemental figures and videos.

[35] P. G. de Gennes, *The Physics of Liquid Crystals* (Oxford University Press, New York, 1975).

[36] A. N. Beris and B. J. Edwards, *Thermodynamics of Flowing Systems* (Oxford University Press, New York, 1994).

[37] S. W. Walker, FELICITY: A MATLAB/C++ toolbox for developing finite element methods and simulation modeling, SIAM J. Sci. Comput. **40**, C234 (2018).

[38] F. M. Leslie, Some constitutive equations for anisotropic fluids, J. Mech. Appl. Math. **19**, 357 (1966).

[39] A. Doostmohammadi, M. F. Adamer, S. P. Thampi, and J. M. Yeomans, Stabilization of active matter by flow-vortex lattices and defect ordering, Nat. Commun. **7**, 10557 (2016).

[40] F. Caballero, Z. You, and M. C. Marchetti, Vorticity phase separation and defect lattices in the isotropic phase of active liquid crystals, Soft Matter **19**, 7828 (2023).

[41] H. Wioland, F. G. Woodhouse, J. Dunkel, and R. E. Goldstein, Ferromagnetic and antiferromagnetic order in bacterial vortex lattices, Nat. Phys. **12**, 341 (2016).

[42] H. Reinken, D. Nishiguchi, S. Heidenreich, A. Sokolov, M. Bär, S. H. L. Klapp, and I. Aranson, Organizing bacterial vortex lattices by periodic obstacle arrays, Commun. Phys. **3**, 76 (2020).

[43] M. L. Blow, S. P. Thampi, and J. M. Yeomans, Biphasic, lyotropic, active nematics, Phys. Rev. Lett. **113**, 248303 (2014).

[44] C. D. Schimming and J. Viñals, Singularity identification for the characterization of topology, geometry, and motion of nematic disclination lines, Soft Matter **18**, 2234 (2022).

[45] C. Nisoli, R. Moessner, and P. Schiffer, Colloquium: Artificial spin ice: Designing and imaging magnetic frustration, Rev. Mod. Phys. **85**, 1473 (2013).

[46] J. Drisko, T. Marsh, and J. Cumings, Topological frustration of artificial spin ice, Nat. Commun. **8**, 14009 (2017).